

Spin Currents and Spontaneous Magnetization at Twin Boundaries of Noncentrosymmetric Superconductors

Emiko Arahata,¹ Titus Neupert,^{2,3} and Manfred Sigrist²

¹*Department of Basic Science, The University of Tokyo,
3-8-1 Komaba, Meguro-ku, Tokyo, 153-8902, Japan*

²*Theoretische Physik ETH-Hönggerberg, CH-8093 Zürich, Switzerland*

³*Condensed Matter Theory Group, Paul Scherrer Institute, CH-5232 Villigen PSI, Switzerland*
(Dated: February 25, 2013)

Twin boundaries are generic crystalline defects in noncentrosymmetric crystal structures. We study theoretically twin boundaries in time-reversal symmetric noncentrosymmetric superconductors that admit parity-mixed Cooper pairing. Twin boundaries support spin currents as a consequence of this parity mixing. If the singlet and triplet components of the superconducting order parameter are of comparable magnitude, the superconducting state breaks spontaneously the bulk time-reversal symmetry locally near the twin boundary. By self-consistently evaluating the Bogoliubov-de Gennes equations and the gap functions we find two distinct phases: First, time-reversal symmetry breaking enhances the spin currents but does not lead to chiral supercurrents. A secondary phase transition then triggers a spin magnetization and an orbital supercurrent near the twin boundary.

Initiated by the discovery of superconductivity in the noncentrosymmetric heavy Fermion compound CePt_3Si , noncentrosymmetric superconductors have opened up new perspectives in the study of unconventional superconductivity [1–9]. Due to the lack of inversion symmetry, these systems feature antisymmetric spin-orbit coupling that breaks completely the $\text{SU}(2)$ spin-rotation symmetry. As a consequence, the superconducting condensate is a superposition of spin-singlet and spin-triplet Cooper pairs [9, 10]. The possibility of realizing different mixing ratios between singlet and triplet pairing is crucial to explore the topological properties of time-reversal symmetric (TRS) noncentrosymmetric superconductors. For example, quasi two-dimensional (2D) superconductors of this kind have a \mathbb{Z}_2 topological attribute when fully gapped (symmetry class DIII in the classification of Ref. [11]). The phases with dominant s -wave pairing (p -wave pairing) are topologically trivial (non-trivial). They are separated by a gap-closing topological phase transition [12]. Akin to the helical electronic edge states of a 2D \mathbb{Z}_2 topological insulator, helical edge modes in the form of Andreev bound states transport a non-conserved spin current along the boundary of a noncentrosymmetric superconductor with dominant p -wave pairing [5, 7, 13–15]. Andreev bound states are a specific signature of unconventional Cooper pairing and directly manifest themselves in tunneling spectroscopy measurements and unique features of spin transport [8].

Very generically, the topology of phases of matter can be probed at defects, such as boundaries, lattice dislocations or vortices in a superconducting order parameter [16]. In noncentrosymmetric materials, the crystal structure allows for another type of defect when two regions of space with the opposite inversion symmetry breaking face each other in a single crystal. In fact, the formation of these so-called twin boundaries is unavoidable in the crystal growth processes of noncen-

trosymmetric materials. A first step towards understanding the parity-mixed superconducting state at intrinsic twin boundaries has been undertaken in Ref. [6]. It revealed that TRS can be spontaneously broken at the twin boundary and that the twin boundary can host vortices with fractional vorticity. The latter offer an explanation for unusually slow flux line dynamics that has been observed experimentally in noncentrosymmetric superconductors [17]: Fractionalized vortices are trapped at the twin boundaries and form an efficient barrier against flux flow.

In this Letter, we develop an extended phenomenology of the possible pairing states at the twin boundary by self-consistently evaluating the Bogoliubov-de Gennes (BdG) equations and the gap functions. We find two distinct phases of broken TRS at the twin boundary. In the first phase, the orbital degrees of freedom of the superconducting order parameter break TRS and enhance the helical spin currents along the twin boundary. Yet, contrary to naive expectations, no chiral current flows despite the broken TRS. This changes with a secondary transition to another TRS broken phase that features both a nonvanishing magnetization and an orbital supercurrent along the twin boundary. In our analysis, we clarify the relation between the bulk topological phase transition and the phase diagram of the states near the twin boundary, as well as the nature and spatial profile of the spin and charge supercurrents in each phase.

We use a tight-binding model describing a 2D noncentrosymmetric superconductor with Rashba spin-orbit coupling that includes pairing interactions based on spin fluctuations, in order to allow for the appearance of unconventional pairing channels. We consider electrons hopping on a square lattice Λ of $L_x \times L_y$ sites $\mathbf{r} = (x, y) \in \Lambda$ that is spanned by the orthogonal unit vectors \mathbf{a}_i , $i = x, y$. The Hamiltonian for the extended Hubbard model including spin-density interactions and

the Rashba spin-orbit coupling [10] reads

$$\begin{aligned}
H := & - \sum_{\mathbf{r}, i} \sum_s c_{\mathbf{r}+\mathbf{a}_i s}^\dagger (t\hat{\sigma}^0 - \boldsymbol{\lambda}_{\mathbf{r}, \mathbf{a}_i} \cdot \hat{\boldsymbol{\sigma}})_{s, s'} c_{\mathbf{r} s'} \\
& + \sum_{\mathbf{r}, i} [J \mathbf{S}_{\mathbf{r}+\mathbf{a}_i} \cdot \mathbf{S}_{\mathbf{r}} + D_{\mathbf{r}, \mathbf{a}_i} \cdot (\mathbf{S}_{\mathbf{r}+\mathbf{a}_i} \times \mathbf{S}_{\mathbf{r}})] \quad (1) \\
& + U \sum_{\mathbf{r}} n_{\mathbf{r}\uparrow} n_{\mathbf{r}\downarrow} + V \sum_{\mathbf{r}, i} n_{\mathbf{r}} n_{\mathbf{r}+\mathbf{a}_i},
\end{aligned}$$

where $c_{\mathbf{r} s}^\dagger$ creates an electron with spin $s = (\uparrow, \downarrow)$ at site $\mathbf{r} \in \Lambda$. The antisymmetric spin-orbit coupling is a Rashba term of strength $\alpha_{\mathbf{r}}$ parametrized by $\boldsymbol{\lambda}_{\mathbf{r}, \mathbf{a}_i} = i\alpha_{\mathbf{r}}(\hat{\mathbf{z}} \times \mathbf{a}_i)$, $i = x, y$, where $\hat{\mathbf{z}}$ is the unit vector normal to the plane of the lattice. The vector $\hat{\boldsymbol{\sigma}} = (\sigma^x, \sigma^y, \sigma^z)$ denotes the three Pauli matrices and $\hat{\sigma}^0$ the 2×2 unit matrix. We define the electron density operator $n_{\mathbf{r} i} = n_{\mathbf{r} i \uparrow} + n_{\mathbf{r} i \downarrow}$ and the spin density operator $\mathbf{S}_{\mathbf{r}} = \sum_{s, s'} c_{\mathbf{r} s}^\dagger \hat{\boldsymbol{\sigma}}_{s, s'} c_{\mathbf{r} s'}$. Besides the ordinary spin-isotropic Heisenberg exchange of strength J , the noncentrosymmetric crystal structure also allows for a Dzyaloshinsky-Moriya type spin-spin interaction of strength $D_{\mathbf{r}}$ which is parametrized as $D_{\mathbf{r}, \mathbf{a}_i} = D_{\mathbf{r}}(\hat{\mathbf{z}} \times \mathbf{a}_i)$, $i = x, y$.

Let us illustrate the mean-field decoupling for a translational invariant system ($\alpha_{\mathbf{r}} \equiv \alpha$, $D_{\mathbf{r}} \equiv D$, $\forall \mathbf{r}$), assuming periodic boundary conditions in both the \mathbf{a}_x and \mathbf{a}_y directions. The Rashba-type spin-orbit interaction breaks the SU(2) spin-rotation symmetry and induces a splitting of the electron bands, with each band exhibiting a specific spin structure in momentum space. At the same time, it allows the gap function to be of mixed parity. Here, we focus on a scenario of mixed s - and a p -wave component for which the BdG mean-field Hamiltonian reads $H^{\text{BdG}} := \sum_{\mathbf{k}} \mathbf{c}_{\mathbf{k}}^\dagger \mathcal{H}_{\mathbf{k}}^{\text{BdG}} \mathbf{c}_{\mathbf{k}}$, with the four-component notation $\mathbf{c}_{\mathbf{k}} = (c_{\mathbf{k}\uparrow}, c_{\mathbf{k}\downarrow}, c_{-\mathbf{k}\uparrow}^\dagger, c_{-\mathbf{k}\downarrow}^\dagger)$ and \mathbf{k} representing the 2D momentum in the Brillouin zone while

$$\mathcal{H}_{\mathbf{k}}^{\text{BdG}} = \begin{pmatrix} \mathcal{H}_{\text{kin}, \mathbf{k}} & \Delta_{\mathbf{k}} \\ \Delta_{\mathbf{k}}^\dagger & -\mathcal{H}_{\text{kin}, -\mathbf{k}}^\top \end{pmatrix}. \quad (2a)$$

The kinetic part of the Hamiltonian is given by

$$\mathcal{H}_{\text{kin}, \mathbf{k}} := -2t[\cos(k_x) + \cos(k_y)]\hat{\sigma}^0 + \mathbf{g}_{\mathbf{k}} \cdot \hat{\boldsymbol{\sigma}}, \quad (2b)$$

with $\mathbf{g}_{\mathbf{k}} := 2\alpha[\hat{x}\sin(k_y) - \hat{y}\sin(k_x)]$. We can decompose the superconducting gap function $\Delta_{\mathbf{k}} = (i\sigma^y)(\Delta_{\mathbf{k}}^{(e)} + \Delta_{\mathbf{k}}^{(o)} \cdot \hat{\boldsymbol{\sigma}})$ in a scalar even parity spin singlet part $\Delta_{\mathbf{k}}^{(e)}$ and a vector odd parity spin triplet part $\Delta_{\mathbf{k}}^{(o)}$ [9, 18]. The assumption of s -wave pairing in the former and p -wave pairing in the latter yields the momentum dependences

$$\Delta_{\mathbf{k}}^{(e)} = \Delta_s^{(e)} (\cos(k_x) + \cos(k_y)) + \Delta_0^{(e)}, \quad (2c)$$

$$\Delta_{\mathbf{k}}^{(o)} = \Delta_p (\sin(k_y), -\sin(k_x), 0). \quad (2d)$$

of the order parameters. Note that the p -wave pairing state with the highest transition temperature is the one with $\Delta_{\mathbf{k}}^{(o)} \propto \mathbf{g}_{\mathbf{k}}$ [9]. This allows to simultaneously diagonalize the gap function and the kinetic part of the

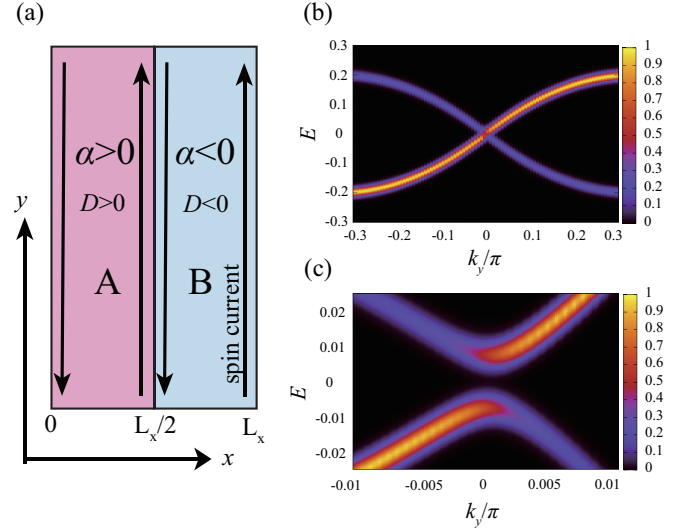


FIG. 1. (Color online) (a) Sketch of the intrinsic metallic interface in a noncentrosymmetric superconductor. If the pairing is dominantly of triplet type, a topologically protected Kramers pair of edge modes carrying a spin current is localized at $x = 0$ and $x = L_x$. Two Kramers pairs of edge modes that are localized near the twin boundary hybridize and thereby lose their topological protection. (b) The spectral function of up-spin quasiparticles at the immediate left of the twin boundary, $A_{x=50, k_y}^{\uparrow}(E)$ shows the spin-polarization of these helical states. The zoom-in (c) reveals their hybridization. ($A_{x=50, k_y}^{\downarrow}(E)$ and $A_{x=51, k_y}^{\uparrow}(E)$ are obtained by flipping the figure about $k_y = 0$.) Parameters are $J = 1.3$, $D = 1.75$, $V = 1.22$, $U = 0.82$, such that $\Delta_s/\Delta_p \sim 0.425$ [19].

Hamiltonian $\mathcal{H}_{\text{kin}, \mathbf{k}}$ by going to the basis of $\lambda = \pm$ helicity states that label the two sheets of the noninteracting band structure. The gap function on either sheet is then given by $\Delta_{\lambda, \mathbf{k}} = \Delta_{\mathbf{k}}^{(e)} + \lambda \Delta_{\mathbf{k}}^{(o)} \cdot \mathbf{g}_{\mathbf{k}}/|\mathbf{g}_{\mathbf{k}}|$, $\lambda = \pm$, making the mixed parity character of the superconducting state explicit.

We now turn to the electronic properties of the system with twin boundary. For that, we equip the Rashba spin-orbit coupling and the Dzyaloshinsky-Moriya interaction in Hamiltonian (1) with the spatial dependencies

$$\alpha_{\mathbf{r}} = \alpha \text{sgn}(x - L_x/2), \quad D_{\mathbf{r}} = D \text{sgn}(x - L_x/2), \quad (3)$$

respectively. This models a twin boundary located at $x = L_x/2$ that separates regions A and B of the superconductor, that have the opposite sign of the Rashba and Dzyaloshinsky-Moriya coupling [see Fig. 1 (a)]. Open and periodic boundary conditions are used in the \mathbf{a}_x and \mathbf{a}_y directions, respectively. In other words, the relative U(1) phase between $\Delta^{(e)}$ and Δ_p has to change by π across the twin boundary. The way the superconducting condensate accommodates this phase twist decisively determines the physics at the twin boundary.

If $\Delta^{(o)}$ is the dominant component of the order parameter, gapless helical edge states exist at the boundary

of a 2D topological superconductor, as dictated by the nontrivial \mathbb{Z}_2 topological index. Localized modes within the bulk spectral gap also exist at the twin boundary, though they would not be endowed with topological protection, for the \mathbb{Z}_2 topological sector of the Hamiltonian is the same on either side. In order to identify the existence and spin polarization of the localized modes at twin boundary, we calculated the spectral function

$$A_{x,k_y}^s(E) = -\frac{1}{\pi} \text{Im} G_{x,k_y}^{s,s}(E), \quad (4)$$

where $G_{x,k_y}^{s,s}$ is the Green's function at position x and momentum k_y . Figures 1(b) and (c) show the spectral function for up-spin quasiparticles on the immediate left of the twin boundary. We observe that the left- and rightgoing modes have opposite spin polarization at high energies and that this spin-momentum locking is lifted with the appearance of a hybridization gap near zero energy.

We are now prepared to report the central results of our analysis on the spontaneous breaking of TRS near the twin boundary. Time-reversal symmetry breaking is signaled by the following two quantities: (i) the relative U(1) phase

$$\varphi := \arg \Delta_{x=L_x/4}^{(e)} - \arg \Delta_{x=3L_x/4}^{(e)} \quad (5)$$

of the singlet component of the superconducting order parameter between regions A and B and (ii) the spin magnetization $M \propto n_{\uparrow} - n_{\downarrow}$ at the twin boundary. To understand the relevance of (i), we have to ask how the condensate can account for the π -shift in the relative U(1) phase between $\Delta^{(e)}$ and Δ_p across the twin boundary. The two values of φ compatible with TRS are $\varphi = 0$ and $\varphi = \pi$. In the former case, $|\Delta^{(e)}| \gg |\Delta^{(o)}|$ and Δ_p accounts for the relative phase shift of π with a sign change by going through zero at the twin boundary. Conversely, if $|\Delta^{(e)}| \ll |\Delta^{(o)}|$, $\Delta^{(e)}$ will change sign and be nodal at the twin boundary, such that $\varphi = \pi$. In contrast, if $|\Delta^{(e)}|$ and $|\Delta^{(o)}|$ are of comparable magnitude, the system is frustrated and the cost in condensation energy for a node in either component at the twin boundary is high. In this case, the relative U(1) phase between $\Delta^{(e)}$ and Δ_p will change continuously from 0 to π across the twin boundary, thereby breaking the TRS locally. This, in turn, is signaled by $\varphi \neq 0, \pi$, where either of the degenerate solutions φ and $-\varphi$ is spontaneously chosen. The phase diagram in Fig. 2 shows that the local TRS breaking at the twin boundary as measured by φ (continuous lines) and the magnetization M (color code) result in two different phase boundaries. We conclude that a secondary phase transition toward the phase labeled C with finite magnetization M arises inside the TRS breaking phase with $\varphi \neq 0, \pi$ labeled B.

For comparison, the dashed lines in Fig. 2(a) define the region in parameter space where the bulk system is gapless due to nodes in the superconducting order parameter.

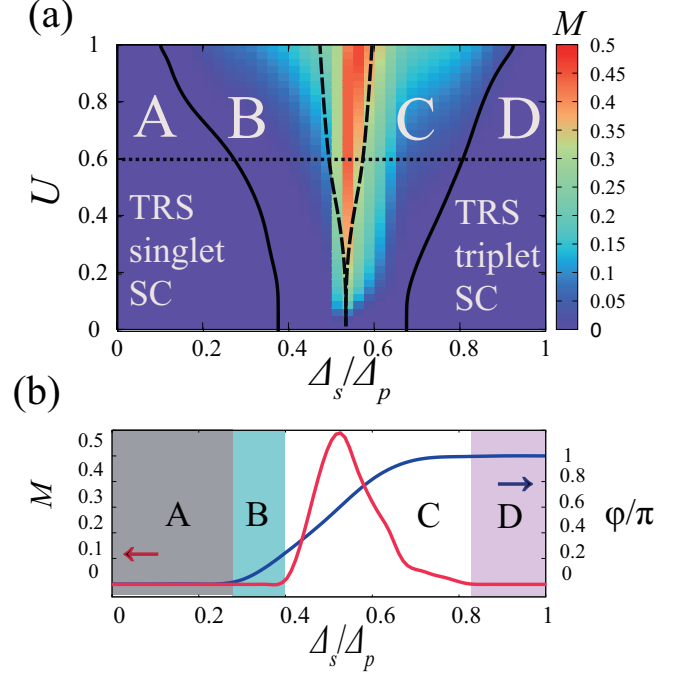


FIG. 2. (Color online) (a) Phase diagram of superconducting and magnetic order at the twin boundary as a function of on-site repulsion U for $J = 1.3$, $D = 1.8$, $V = 1.2$ [19]. Continuous lines separate phases of (A) TRS singlet dominated superconductivity, (B,C) TRS breaking phase where the φ deviates from the values 0 and π near the twin boundary, and (D) TRS triplet dominated superconductivity. The color scale measures the spin magnetization near the twin boundary that becomes nonzero in phase (C) via a secondary phase transition in the phase with broken TRS. Dashed lines encircle the region in parameter space where the bulk superconducting gap is nodal, marking the topological phase transition from the trivial (left) to the nontrivial (right) \mathbb{Z}_2 topological superconductor. (b) Spin-magnetization M and phase φ along the dotted line in (a).

Left (right) of this region, the bulk is a topologically trivial (non-trivial) superconductor. The topological phase transition acquired a finite width due to the term $\Delta_s^{(e)}$ in the Hamiltonian. Inside the gapless region, the order parameter has several point nodes on the Fermi surfaces. In the edge Brillouin zone, flat edge bands stretch between the projections of pairs of these nodal points, much like the surface flatbands in graphene zigzag edges. We make the following two observations that relate to these topological features. First, the bulk topological phase transition happens fully inside the parameter range in which TRS is spontaneously broken at the twin boundary. Second, the magnetic order at the twin boundary is strongly enhanced in the bulk gapless region. This can be attributed to Stoner-like magnetism of the edge flatbands at the twin boundary.

Finally, let us study how the spontaneous TRS breaking manifests itself in the (spin) Hall response at the twin

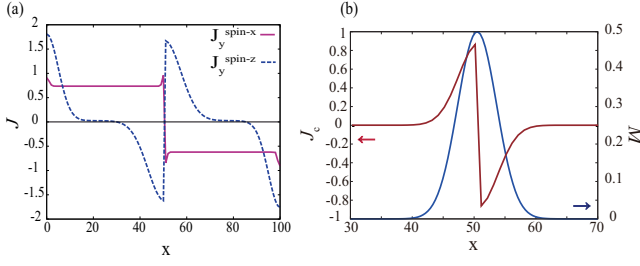


FIG. 3. (Color online) (a) Spin current in the y direction as a function of x . The solid lines and the dashed lines are the spin currents with spin polarization in the x and y direction, respectively. Parameters are $J = 1.1$, $D = 2.0$, $V = 1.5$, $U = 0.87$, such that $\Delta_s/\Delta_p = 0.41$ [19]. (b) The x -dependence of the orbital supercurrent (red line) and of the magnetization (blue line) near the twin boundary in the TRS broken phase. Parameters are $J = 1.3$, $D = 2.1$, $V = 1.2$, $U = 0.87$, such that $\Delta_s/\Delta_p = 0.5$ [19].

boundary. For that, we define the spin current of polarization $i = x, y, z$ that runs in the y -direction

$$J_y^{\text{spin}-i}(x) := \text{Tr} \sum_{k_y} c_{k_y,x}^\dagger \left(\partial_{k_y} \mathcal{H}_{k_y,x}^{\text{BdG}} \right) \hat{\sigma}^i c_{k_y,x}, \quad (6)$$

where the trace is taken over all states below zero energy. We show in Fig. 3(a) the spin currents $J_y^{\text{spin}-x}$ and $J_y^{\text{spin}-z}$ as a function of position x inside the phase B of phase diagram 2(a). Each of them has opposite signs on either side of the twin boundary. The component $J_y^{\text{spin}-y}$ vanishes in the bulk and is much smaller than $J_y^{\text{spin}-z}$ at the twin boundary (not shown). The component $J_y^{\text{spin}-z}$ corresponds to the usual spin current carried by an Andreev bound states and is similar at the edge of the sample and at the twin boundary. The component $J_y^{\text{spin}-x}$ is finite also in the bulk and increases at the boundary. However, its bulk contribution should not be interpreted as a physically measurable spin current [20]. The form of the boundary contribution of the spin current is governed by the length scale that the spin-orbit coupling α introduces, namely the inverse difference between the Fermi momenta of the spin-orbit split Fermi surfaces $1/|k_{F+} - k_{F-}|$. If this length scale becomes smaller than the coherence length that governs the decay of the spin current towards the bulk, oscillations appear in $J_y^{\text{spin}-x}$ (not shown in Fig. 3). The phase C of phase diagram 2(a) is characterized by the finite magnetization M shown in Fig. 3(b). This magnetization is accompanied by a orbital supercurrent that runs in opposite directions on the immediate left and right of the twin boundary [Fig. 3(b)].

In summary, we studied the superconducting interface states between twin domains in a mixed-parity superconductor by evaluating the BdG equations and the gap functions self-consistently. We find that the breaking of inversion symmetry, the superconducting order, and the

proximity to a topological phase transition can combine in a nontrivial way to create a phase of spontaneously broken TRS at the interface. The twin boundary either hosts a spin current or carries a chiral supercurrent along with a spontaneous spin magnetization. The TRS breaking phase is intimately connected with the bulk topological phase transition.

In closing, we note that the mechanism for TRS breaking that we discussed in this work is not limited to twin boundaries in noncentrosymmetric superconductors. It can also be of relevance to tunable devices with interface superconductivity such as $\text{SrTiO}_3/\text{LaAlO}_3$, if the Rashba spin-orbit coupling is not uniform in space [21]. A similar phenomenology might apply to other ordering phenomena, such as the spontaneous generation of the quantum spin Hall effect in graphene-like materials [22]. In this case, TRS may be broken at the boundary between regions of opposite spin-Hall conductivity, spontaneously generating a charge Hall effect.

This work was supported in part by the Swiss National Science Foundation. E. A. was supported by a Grant-in-Aid from JSPS.

-
- [1] E. Bauer, G. Hilscher, H. Michor, C. Paul, E. Scheidt, A. Griбанov, Y. Seropegin, H. Noël, M. Sigrist, and P. Rogl, Phys. Rev. Lett. **92**, 027003 (2004).
 - [2] P. A. Frigeri, D. F. Agterberg, A. Koga, and M. Sigrist, Phys. Rev. Lett. **92**, 097001 (2004).
 - [3] Y. Yanase and M. Sigrist, J. Phys. Soc. Jpn. **76**, 043712 (2007).
 - [4] T. Yokoyama, S. Onari, and Y. Tanaka, Phys. Rev. B **75**, 172511 (2007).
 - [5] M. Sato and S. Fujimoto, Phys. Rev. B **79**, 094504 (2009).
 - [6] C. Inotakis, S. Fujimoto, and M. Sigrist, J. Phys. Soc. Jpn. **77**, 083701 (2008).
 - [7] C. Lu and S. Yip, Phys. Rev. B **82**, 104501 (2009).
 - [8] A. B. Vorontsov, I. Vekhter, and M. Eschrig, Phys. Rev. Lett. **101**, 127003 (2008).
 - [9] E. Bauer and M. Sigrist, *Non-centrosymmetric Superconductors - Introduction and Overview* (Springer, New York, 2012).
 - [10] L. P. Gor'kov and E. I. Rashba, Phys. Rev. Lett. **87**, 037004 (2001).
 - [11] A. P. Schnyder, S. Ryu, A. Furusaki, and A. W. W. Ludwig, Phys. Rev. B **78**, 195125 (2008), URL <http://link.aps.org/doi/10.1103/PhysRevB.78.195125>.
 - [12] L. Santos, T. Neupert, C. Chamon, and C. Mudry, Phys. Rev. B **81**, 184502 (2010), URL <http://link.aps.org/doi/10.1103/PhysRevB.81.184502>.
 - [13] Y. T. et al., Phys. Rev. B **79**, 060505(R) (2009).
 - [14] C. I. et al., Phys. Rev. B **76**, 012501 (2007).
 - [15] T. Yokoyama, Y. Tanaka, and J. Inoue, Phys. Rev. B **72**, 220504(R) (2005).
 - [16] J. C. Y. Teo and C. L. Kane, Phys. Rev. B **82**, 115120 (2010), URL <http://link.aps.org/doi/10.1103/PhysRevB.82.115120>.

- [17] H. Mukuda, S. Nishide, A. Harada, K. Iwasaki, M. Yogi, M. Yashima, Y. Kitaoka, M. Tsujino, T. Tkeuchi, R. Setta, et al., J. Phys. Soc. Jpn. **78**, 014705 (2009).
- [18] M. Sigrist and K. Ueda, Rev. Mod. Phys. **63**, 239 (1991).
- [19] Throughout this paper, we set $\alpha = 1$, $L_x = 100$ and fix the electron density per lattice site to $n = 0.9$, while we change the parameters of the interaction U , V , J , and D as appropriate. All energies are measured in units of t .
- [20] E. I. Rashba, Phys. Rev. B **68**, 241315 (2003), URL <http://link.aps.org/doi/10.1103/PhysRevB.68.241315>.
- [21] N. Reyren, S. Thiel, A. D. Caviglia, L. F. Kourkoutis, G. Hammerl, C. Richter, C. W. Schneider, T. Kopp, A.-S. Ruetschi, D. Jaccard, et al., Science **317**, 1196 (2007), ISSN 0036-8075.
- [22] S. Raghu, X.-L. Qi, C. Honerkamp, and S.-C. Zhang, Phys. Rev. Lett. **100**, 156401 (2008), URL <http://link.aps.org/doi/10.1103/PhysRevLett.100.156401>.